J Electroceram (2014) 33:128–133
DOI 10.1007/s10832-014-9951-z

Improvement of piezoelectric and ferroelectric properties in (K,Na)NbO_3- based ceramics via microwave sintering

Mohammad Reza Bafandeh · Raziyeh Gharahkhani · Mohammad Hasan Abbasi · Ali Saidi · Jae-Shin Lee · Hyoung-Su Han

Received: 29 November 2013 / Accepted: 30 May 2014 / Published online: 13 June 2014

Abstract In this study modified KNN–based piezoceramics with different amounts of $SrTiO_3$ were prepared. Sintering was carried out in a conventional furnace (via single–step as well as two–step sintering) and in a microwave furnace. Sintering behavior, piezoelectric properties, ferroelectric and strain behavior of sintered samples were investigated. Observation of microstructures proved that two–step sintering suppressed grain growth and enhanced densification. Microwave sintered samples exhibited the highest piezoelectric constant compared to the other samples which might be attributed to higher density and lower loss of volatile elements such as K and Na during microwave sintering. Microwave sintering also resulted in the improvement of ferroelectric behavior and enhancement of electric–field–induced strain. This work demonstrates the potential of microwave sintering to fabricate KNN–based ceramics with better electromechanical properties compared to those obtained using conventional furnace sintering.

Keywords Sodium potassium niobate · Lead-free ceramics · Microwave sintering · Piezoelectric properties · Ferroelectric properties

M. R. Bafandeh
Department of Metallurgy, University of Kashan, Kashan, Iran

R. Gharahkhani · M. H. Abbasi · A. Saidi
Department of Materials Engineering, Isfahan University of Technology (IUT), Isfahan 84156-83111, Iran

J.-S. Lee · H.-S. Han (✉)
School of Materials Science and Engineering, University of Ulsan, Ulsan, Republic of Korea
e-mail: hsejs@ulsan.ac.kr

1 Introduction

Lead–free perovskite materials have been extensively studied for exploring alternatives to lead–based piezoelectrics due to legislative regulations such as RoHS and WEEE [1]. One of candidates is sodium potassium niobate (KNN) which exhibits relatively good piezoelectric properties and high Curie temperature [2]. Poor sinterability and volatilization of sodium and potassium during sintering are the main factors that make them difficult in mass production with reproducibility [3–5].

So far different ways to obtain dense KNN–based ceramics have been proposed and examined. Some of researchers [6–9] improved sintering behavior by using sintering aids. Recently Li et al. [10] well demonstrated about KNN–based materials.

The limitation of sintering aids is their probable negative effect on ferroelectric and piezoelectric properties of prepared ceramics. The sintering behavior was also reported to be affected by composition modification, i.e., adding dopants [11–13] or modifiers [14, 15]. The other way to obtain dense ceramics is sintering via novel sintering methods such as hot pressing [16, 17] and spark plasma sintering [18, 19]. However these methods are complex and expensive, which makes them difficult in industrial application.

Recently two step sintering (TSS) using a conventional furnace has been reported to enhance densification as well as to suppress grain growth [20–22]. In the first step of TSS, the sample is kept at higher temperature (T_1) for a short time span to reach a critical density and then rapidly cooled down to a lower temperature (T_2), soaking for relatively prolonged time to densify without grain growth [20]. Due to TSS potential in decreasing the required sintering temperature effectively, this method can be used to sinter compounds containing volatile elements [23, 24]. As a result, the loss of volatile elements is eliminated or at least is decreased while improving sintered density. So far, using TSS for sintering KNN–based

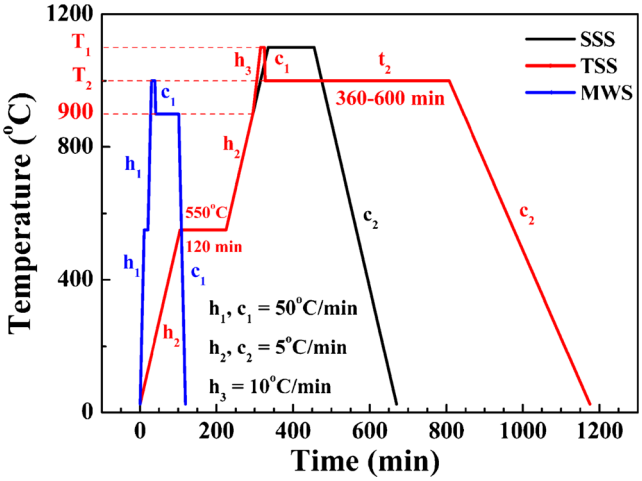

Fig. 1 Time–temperature profiles for single–step sintering (SSS) and two–step sintering (TSS) using a conventional electric furnace, and rapid thermal processing using a microwave furnace, so called, microwave sintering (MWS)

compounds has not been studied so much even though there has been a couple of reports [25, 26].

One of sintering methods that can significantly reduce sintering temperature and time is microwave sintering (MWS) [27]. In this method heat is generated inside the material instead of heat transfer to sample in conventional furnace. Application of MWS to compounds containing volatile elements could decrease volatilization and improve densification [28, 29]. According to above-mentioned advantages for TSS, it seems that combination of this sintering route with microwave sintering effectively enhance densification and suppress elements loss during sintering.

The aim of this work is improvement sinterability and properties of KNN-based ceramics via TSS and MWS. Therefore in this work, $(1–x)$ $(K_{0.48}Na_{0.48}Li_{0.04})(Nb_{0.96}Ta_{0.04})O_3$ – $xSrTiO_3$ (abbreviated as $(1–x)$KNNLT – xST) compounds were sintered via three different methods, single step sintering (SSS), two step sintering (TSS) and microwave sintering (MWS). This work compared the microstructure, piezoelectric properties, ferroelectric and strain behavior of KNNLT–ST ceramics prepared via three different sintering methods.

2 Experimental

$(1–x)$ KNNLT – xST $(0 \leq x \leq 0.10)$ powders were synthesized by a conventional solid state reaction method using Na_2CO_3, K_2CO_3, Li_2CO_3, Nb_2O_5, Ta_2O_5, SrO and TiO_2 with more than 99 % purity as raw materials. At first, these powders were dried in an oven at 100 °C for 24 h and then were weighed for

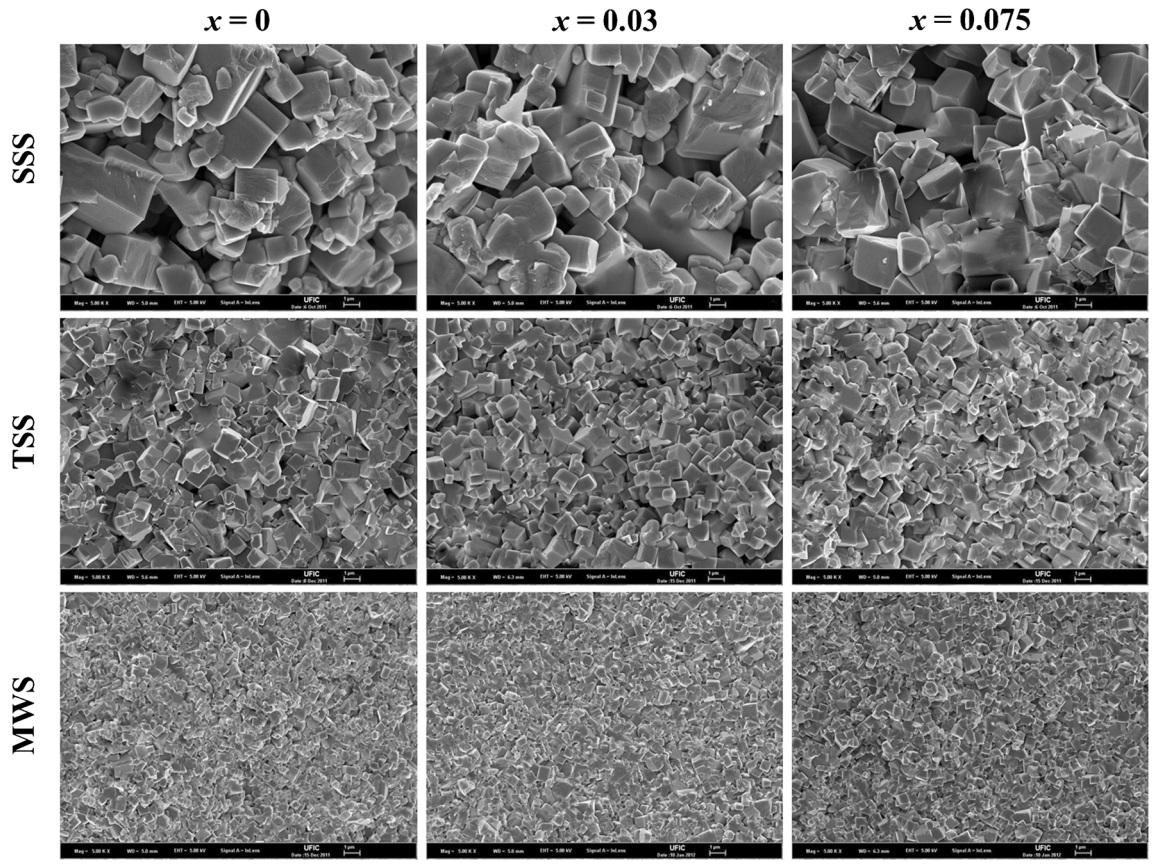

Fig. 2 SEM images of $(1–x)$KNNLT – xST ceramics optimally prepared via SSS, TSW, and MWS

each composition according to the stoichiometric formula. Each powder mixture was ball–milled for 24 h with zirconia balls using ethanol media. The dried slurries were calcined at 880 °C for 6 h. In order to increase composition homogeneity, the calcination was carried out twice separated by 24 h ball milling. Calcined powders were mixed with polyvinyl alcohol as a binder and then pressed into green disks with a diameter of 12 mm at 98 MPa. Green disks were sintered via three different routes; conventional single–step sintering (SSS), TSS, and MWS. A multimode 2.45 GHz microwave furnace with a power output of 3 kW was used in MWS. Temperature cycles in SSS, TSS and MWS procedures are compared in Fig. 1. For SSS, the samples were sintered in the range 1060–1150 °C for 2 h. For TSS, samples were sintered in the range 1060–1140 °C as T_1 for 10 min and 1000–1040 °C as T_2 for 6–10 h. For MWS, samples were sintered in the range 950–1050 °C as T_1 for 10 min and 850–950 °C as T_2 for 30–120 min.

The Archimedes method was used to measure the density of sintered ceramics. The temperature that yielded the maximum relative density for each composition was selected as the optimum sintering temperature. The microstructure of ceramics was observed using a scanning electron microscope (FE–SEM, JEOL, JSM–65OFF, Japan). The crystal structure of samples was determined using an X–ray diffractometer (XRD, X'pert PRO MRD, Philips). For electrical measurements, silver paste was applied on the lapped surfaces of the disks to serve as the electrodes. The polarization versus electric field hysteresis loop was measured using a Sawyer–Tower circuit to apply an electric field with a triangular waveform. The electric–field–induced strain (EFIS) was measured using a linear variable differential transducer (LVDT, Mitutoyo MCH–331 & M401). The voltage was supplied using a high voltage amplifier (Trek, 610E) driven by a waveform generator (Agilent 33250A). Poling was carried out at 100 °C in silicon oil bath by applying an electric field of 3–4 kV/mm for 30 min. The piezoelectric constant (d_{33}) was measured using a piezo–d_{33} meter (ZJ–6B, China).

3 Results and discussion

FE-SEM images of (1–x) KNNLT – xST compounds which were optimally sintered via SSS, TSS and MWS are shown in Fig. 2. As can be seen in the Fig. 2, SSS resulted in relatively porous microstructure containing large and nonuniform grains, while TSS suppressed grain growth effectively and improved densification. This phenomenon might be related with the influences of TSS on related mechanisms to grain growth and densification [20]. Sintering in a microwave furnace more effectively retarded grain growth with higher densities probably due to higher heating rate. Densities of optimally sintered ceramics via SSS, TSS and MWS are compared

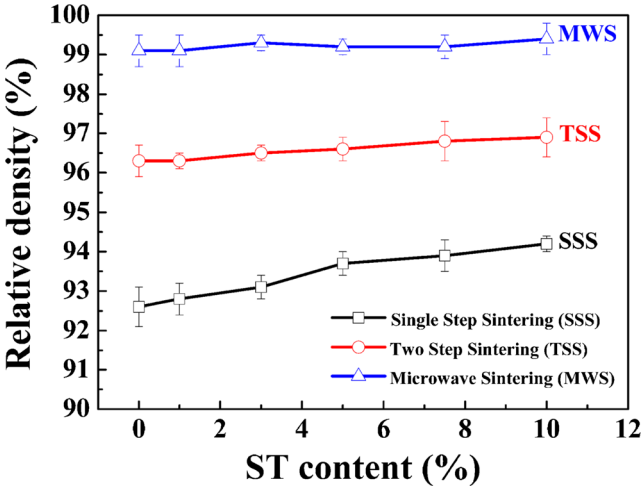

Fig. 3 Relative density of (1–x)KNNLT – xST ceramics prepared via SSS, TSS and MWS as a function of ST content

in Fig. 3. It can be seen that the maximum density for KNNLT sintered via SSS and TSS are about 93 and 96 % of the theoretical density (TD), respectively, while MWS resulted in 99 % of TD.

X–ray diffraction (XRD) patterns of (1–x) KNNLT – xST ceramics sintered at optimum sintering temperatures via SSS are shown in Fig. 4. By comparing XRD patterns with JCPDS pattern 01–071–2171 (corresponding to orthorhombic $KNbO_3$) and 01–071–0945 (corresponding to tetragonal $KNbO_3$) it was found that all samples showed pure perovskite structure without any secondary phase, indicating formation of solid solution between KNNLT and ST within the studied range $0 \le x \le 0.10$. XRD patterns of ceramic with $x=0$ shows (202)/(020) peak splitting at around $2\theta=46°$, confirming the orthorhombic symmetry. This observation is in good agreement with reported results by Guo et al. [30]. For specimens with $0.03 \le x \le 0.075$, XRD patterns show (002)/(200) peak splitting, indicating the tetragonal symmetry. The split peaks at around $2\theta=46°$ in XRD pattern of ceramic with $x=0.01$ have equal intensities due to the coexistence of orthorhombic and tetragonal structures. The merging of the split peaks

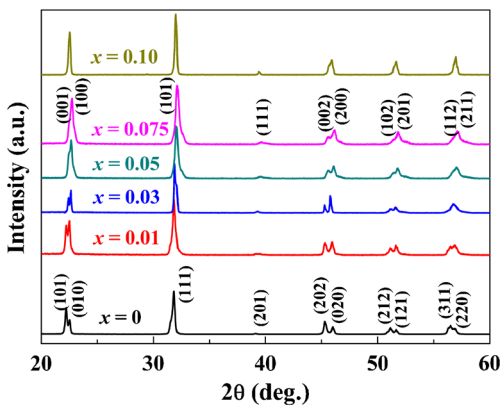

Fig. 4 XRD patterns of (1–x)KNNLT – xST ceramics

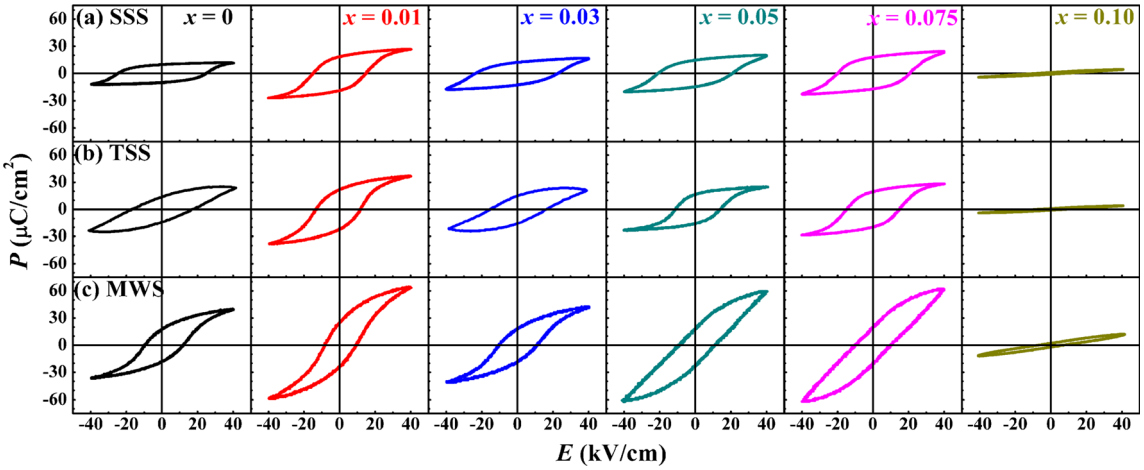

Fig. 5 *P–E* hysteresis loops of (1–*x*)KNNLT – *x*ST ceramics prepared via (a) SSS, (b) TSS, and (c) MWS, respectively

together for a sample with x=0.10 indicates formation of pseudocubic structure. By comparing the peak angles of different compositions, it can be found that with increasing ST amount, the diffraction peaks shift toward higher angles, indicating the shrinkage of unit cell. This result seems to be due to the smaller ionic radius of Sr^{2+} ions (1.44 Å, CN=12) compared to the average ionic radius of A–site matrix ions, i.e. Na^{+} (1.39 Å, CN=12) and K^{+} (1.64 Å, CN=12), as well as the smaller Ti^{4+} ion (0.61 Å, CN=6) compared to Nb^{5+} (0.64 Å, CN=6) which is the matrix B–site ion in the ABO_3 perovskite structure. It should be noted that XRD patterns of sintered ceramics via TSS and MWS were similar to those of SSS–derived counterparts.

In order to investigate ferroelectric properties of sintered ceramics, variations of their polarizations versus applied electric field were plotted. Two important parameters which can be extracted from *P–E* loops are remenant polarization (P_r) and coercive field (E_c). P_r is due to remained parallel dipole vectors of domains after removing electric field and E_c is required electric field for 180° domain switching.

Figure 5 compares *P–E* hysteresis loops of KNNLT–ST ceramics obtained by using three different sintering routes. All specimens exhibited definite P_r and E_c values, indicating ferroelectricity except 10 mol% ST ceramics. Since the crystal structure of the specimen with x=0.10 is pseudocubic, it is nonpolar and as a result its remenant polarization is not higher than 1 μC/cm^2. The maximum P_r and minimum E_c was observed in a ceramic containing 1 mol% ST because of coexistence of orthorhombic and tetragonal structures, leading to increased possible domain switching directions.

With increasing ST content from 3 to 7.5 mol%, P_r increased but E_c decreased. Investigation of the variations of P_r and E_c as a function of ST content revealed that the trend for MWS–derived ceramics corresponded to those of SSS and TSS–derived ones as shown in Fig. 6a and b. Moreover the MWS–derived ceramics showed higher P_r and lower E_c as compared to other ceramics. Higher density and lower alkali elements loss for MWS–derived ceramics may be responsible for this observation.

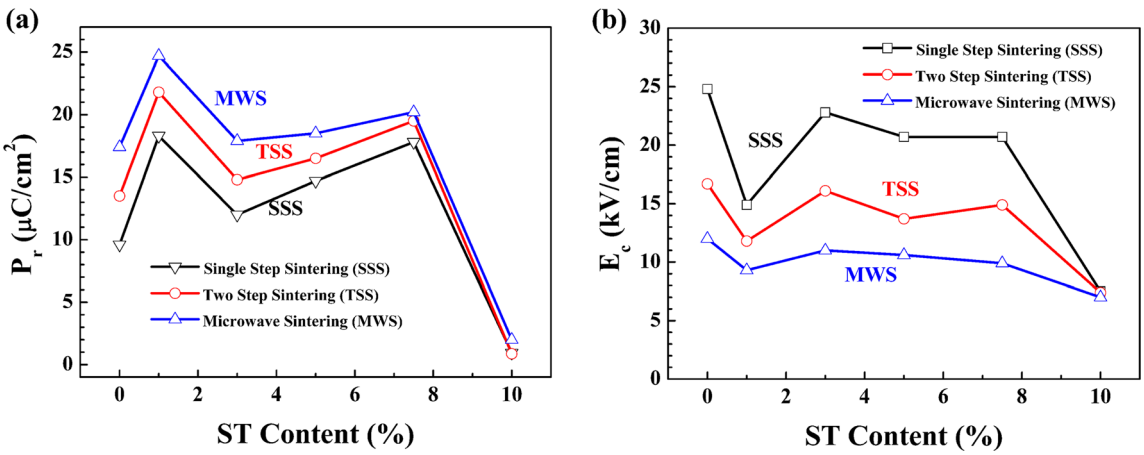

Fig. 6 (**a**) Remanent polarization (P_r) and (**b**) coercive field (E_c) as a function of x in (1–x)KNNLT – xST ceramics

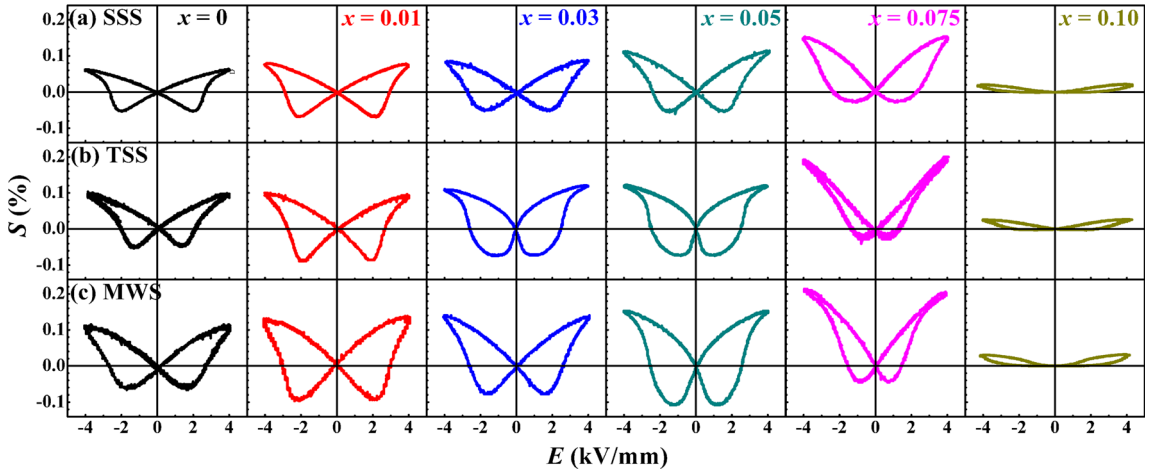

Fig. 7 Bipolar electric–field–induced strain of (1–*x*)KNNLT – *x*ST ceramics prepared via (**a**) SSS, (**b**) TSS, and (**c**) MWS, respectively

Figure 7 presents bipolar strain loops of SSS, TSS and MWS–derived ceramics. The existence of negative strain (S_{neg}) for all samples except a ceramic containing 10 mol% ST implies 90° domain switching during variation of applied electric field. For ceramic with x=0.10, the negative strain is not observed which is due to lack of domain switching in a pseudocubic structure.

The specimen with x=0.075 showed lower negative strain than samples with x<0.075. This is probably due to existence some regions in this ceramic with local composition close to that of 0.90KNNLT–0.10ST. This compositional inhomogeneity is may be caused by the formation of local nonpolar regions with pseudocubic structure that reduces S_{neg}. Reduction in S_{neg} of ceramic with x=0.075 is accompanied by an increase in its S_{max}. Nevertheless existence of nonpolar local regions with pseudocubic structure in 0.925KNNLT–0.075ST, the predominant phase is polar tetragonal phase and is responsible for strain behavior. Electric–field–induced transformation from nonpolar to ferroelectric also affects strain behavior, resulting in an increased strain of ceramic with x=0.075 as compared to other compounds composed of only ferroelectric phase ($x \leq 0.05$). In other words, the sudden increase in strain of ceramic with x=0.075 is due to simultaneous effect of EFIS as well as electric–field–induced transformation from nonpolar to polar phase. This phenomenon is similar with the giant strain of Bi–based ceramics [31, 32].

In the specimen with x=0.10, pseudocubic nonpolar phase is predominant and a drastic deviation from typical behavior of ferroelectric materials (butterfly curve) and lack of S_{neg} is observed. The variations of unipolar strain as a function of applied electric field for SSS, TSS and MWS–derived ceramics were studied. Dynamic piezoelectric constant or normalized strain (d^*_{33}) of different sintered ceramics which is calculated from the ratio between the S_{max} in unipolar curve and its related electric field, are compared in Fig. 8. By comparison of the observed strain between samples sintered via SSS, TSS and MWS, it can be concluded MWS–derived samples show higher strain under same applied electric field, which can be attributed to denser, more uniform microstructures with lower loss in alkali elements during thermal process in MWS–derived ceramics.

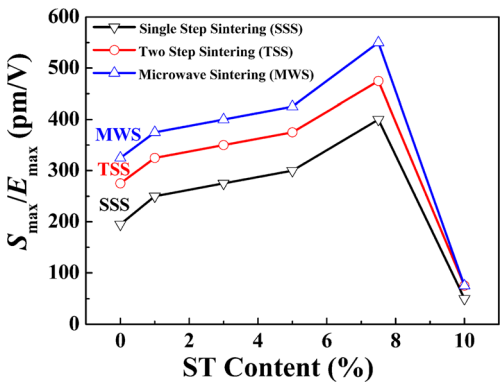

Fig. 8 Dynamic piezoelectric constant of (1–*x*)KNNLT – *x*ST ceramics prepared via SSS, TSS and MWS as a function of ST content

4 Conclusions

In this work, we compared the microstructure, ferroelectric and piezoelectric properties of KNN–based compounds sintered in a microwave furnace, as well as in a conventional furnace (either via single–step or two–step). Observation of microstructures proved that MWS suppressed grain growth and enhanced densification which might be attributed to higher density and lower loss of volatile elements such as K and Na during MWS. This behavior is responsible for improvement of piezoelectric properties, ferroelectric and strain behavior in MWS–derived samples than SSS and TSS–derived ones. Moreover TSS compared to SSS could decrease sintering temperature and increase density of ceramics, resulting in enhanced piezoelectric properties.

Acknowledgment M.R. Bafandeh thanks the financial support of University of Kashan to carry out this work. J.–S. Lee thanks the financial support from the National Research Foundation, Republic of Korea, under the contract No.2013R1A1A2058917.

References

1. E. Ringgaard, T. Wurlitzer, J. Eur. Ceram. Soc. **25**, 2701 (2005)
2. T. Takenaka, H. Nagata, Y. Hiruma, Jpn. J. Appl. Phys. **47**, 3787 (2008)
3. L. Egerton, D.M. Dillon, J. Am. Ceram. Soc. **42**, 438 (1959)
4. R.C. Chang, S.Y. Chu, Y.F. Lin, C.S. Hong, P.C. Kao, C.H. Lu, Sens. Actuators A **138**, 355 (2007)
5. H. Birol, D. Damjanovic, N. Setter, J. Eur. Ceram. Soc. **26**, 861 (2006)
6. Y.M. Li, Z.Y. Shen, Z.G. Xiao, Z.M. Wang, W.Q. Luo, Y. Hong, R.H. Liao, J. Electroceram. **31**, 42 (2013)
7. S.L. Yang, C.C. Tsai, C.S. Hong, S.Y. Chu, Mater. Res. Bull. **47**, 998 (2012)
8. J.G. Fisher, A. Bencan, J. Godnjavec, M. Kosec, J. Eur. Ceram. Soc. **28**, 1657 (2008)
9. M. Matsubara, T. Yamaguchi, K. Kikuta, S.I. Hirano, Jpn. J. Appl. Phys. **44**, 6618 (2005)
10. J.F. Li, K. Wang, F.Y. Zhu, L.Q. Cheng, F.Z. Yao, J. Am. Ceram. Soc. **96**, 3677 (2013)
11. R. Saravanan, D. Rajesh, S.V. Rajasekaran, R. Perumal, M. Chitra, R. Jayavel, AIP Conference Proceedings **1536**, 863 (2013)
12. I.Y. Kang, I.T. Seo, U.J. Cha, J.H. Choi, S. Nham, T.H. Sung, J.H. Paik, J. Eur. Ceram. Soc. **32**, 2381 (2012)
13. Y. Huan, X. Wang, L. Guo, L. Li, J. Am. Ceram. Soc. **96**, 3470 (2013)
14. S. Su, R. Zuo, X. Wang, L. Li, Mater. Res. Bull. **45**, 124 (2010)
15. H. Wang, X. Zhai, J. Xu, C. Yuan, C. Zhou, J. Mater, Sci.- Mater. Electron. **24**, 2469 (2013)
16. M. Ichiki, L. Zhang, M. Tanaka, R. Maeda, J. Eur. Ceram. Soc. **24**, 1693 (2004)
17. J.G. Fisher, A. Bencan, M. Kosec, S. Vernay, D. Rytz, J. Am. Ceram. Soc. **91**, 1503 (2008)
18. J.F. Li, K. Wang, B.P. Zhang, L.M. Zhang, J. Am. Ceram. Soc. **89**, 706 (2006)
19. Y. Zhen, J.F. Li, K. Wang, Y. Yan, L. Yu, L. Mater, Sci. Eng. B: Solid-State Materials for Advanced Technology **176**, 1110 (2011)
20. I.W. Chen, X.H. Wang, Nature **404**, 168 (2000)
21. Y. Xiong, J. Hu, Z. Shen, J. Eur. Ceram. Soc. **33**, 2087 (2013)
22. M. Mazaheri, A.M. Zahedi, S.K. Sadrnezhaad, J. Am. Ceram. Soc. **91**, 56 (2008)
23. J. Fang, X. Wang, L. Li, Key Eng. Mater. **512–515**, 372 (2012)
24. W. Meng, R. Zuo, S. Su, X. Wang, L. Li, J. Mater, Sci.- Mater. Electron. **22**, 1841 (2011)
25. X. Pang, J. Qiu, K. Zhu, J. Du, Ceram. Int. **38**, 2521 (2012)
26. J. Hao, W. Bai, B. Shen, J. Zhai, J. Alloys Compd. **534**, 13 (2012)
27. M. Oghbaei, O. Mirzaee, J. Alloys Compd. **494**, 175 (2010)
28. M. Feizpour, H. Barzegar Bafrooei, R. Hayati, T. Ebadzadeh, Ceram. Int. **40**, 871 (2013)
29. K. Yan, K. Matsumoto, T. Karaki, M. Adachi, J. Am. Ceram. Soc. **93**, 3823 (2010)
30. Y. Guo, K. Kakimoto, H. Ohsato, Mater. Lett. **59**, 241 (2005)
31. W. Jo, R. Dittmer, M. Acosta, J. Zang, C. Groh, E. Sapper, K. Wang, J. Rödel, J. Electroceram. **29**, 71 (2012)
32. H.S. Han, W. Jo, J.K. Kang, C.W. Ahn, I.W. Kim, K.K. Ahn, J.S. Lee, J. Appl. Phys. **113**, 154102 (2013)